Catal Lett (2012) 142:1202–1210
DOI 10.1007/s10562-012-0876-3

Photocatalytically Reducing CO_2 to Methyl Formate in Methanol Over Ag Loaded $SrTiO_3$ Nanocrystal Catalysts

Dandan Sui · Xiaohong Yin · Hongzhi Dong · Shiyue Qin · Jingshuai Chen · Wanlin Jiang

Received: 6 April 2012 / Accepted: 15 July 2012 / Published online: 2 August 2012

Abstract Ag–$SrTiO_3$ nanocrystal photocatalysts were prepared by hydrothermal synthesis method for reducing CO_2 to methyl formate (MF) in methanol via ultraviolet irradiation. CO_2 was reduced to MF by electrons on conduction band of the photocatalyst. In order to obtain a high rate of MF evolution, we researched and optimized the preparation procedure of Ag–$SrTiO_3$ by changing the Ag dosage, hydrothermal temperature and time. The as synthesized photocatalysts were characterized with X-ray diffraction, UV–Vis absorption spectra, transmission electron microscope, N_2 sorption analysis at 77 K and activity evaluation. A catalyst of 7 wt% Ag on $SrTiO_3$ with hydrothermal synthesis at 150 °C and 22 h was found to exhibit the highest photocatalytic activity in MF formation rate of 3,006 μmol/(h g cat), which was more remarkable than that of pristine $SrTiO_3$.

Keywords Photocatalysis · Reduction of CO_2 · Ag–$SrTiO_3$ · Hydrothermal synthesis · Methanol · Methyl formate

1 Introduction

The combustion of the fossil fuel has led to a sharp increase in CO_2 emission, and then resulted in worsening greenhouse effect, which has attracted the worldwide attention. Many efforts have been made to reduce the amount of carbon dioxide in the atmosphere, such as converting CO_2 to dissolved carbonate in sea water, capturing CO_2 and transferring it to the bottom of the sea in a supercritical state [1]. Meanwhile, the exploration of new energy is urgent, due to the increasing lack of fuel resources. The solar energy has become a feasible way to solve the problems by using the sustainable energy of sunlight to capture and convert CO_2 in atmosphere to valuable chemicals, which will prohibit global warming and sustainable energy shortage simultaneously. Photocatalysis is dominated by photocatalysts, such as semiconductor of metal oxides like TiO_2, CdS, ZrO_2, ZnO, and MgO, which have been studied. Among them, nanostructured TiO_2 is one of the most promising photocatalytic materials in terms of its cost and stability [2–6]. Meanwhile, the research is also focus on the design and preparation of perovskite nanostructured photocatalysts due to their ferroelectricity, superconductivity, high dielectric constant, and thermal stability. Strontium titanate ($SrTiO_3$) has a typical Perovskite structure, as a potential photocatalyst, $SrTiO_3$ and metal-loaded $SrTiO_3$ have been effectively utilized in water decomposition and degradation of dye compounds under ultraviolet (UV) radiation [7–13].

In this paper, we used the hydrothermal method to synthesize the Ag-loaded $SrTiO_3$ nanocrystal photocatalysts, where Ag site acted as the electron acceptor to avoid the recombination of electrons and holes, and result in effective extension of the life-span of the electron–hole pairs. The as prepared photocatalysts enhanced the photocatalytic activity remarkably in reducing CO_2.

2 Experimental

2.1 Preparation of Photocatalysts

Ag-loaded $SrTiO_3$ powder was prepared by hydrothermal synthesis. All reagents were used as received from Tianjin

D. Sui · X. Yin (✉) · H. Dong · W. Jiang
School of Chemistry and Chemical Engineering,
Tianjin University of Technology, Tianjin 300384, China
e-mail: xiaohongyin@hotmail.com

S. Qin · J. Chen
School of Chemical Engineering and Technology,
Tianjin University, Tianjin 300072, China

Benchmark Chemical Reagent Co., Ltd of China without further purification. The Ag–$SrTiO_3$ was synthesized as follows: strontium nitrate [$Sr(NO_3)_2$, 99.5 %] and silver nitrate ($AgNO_3$, 99 %) were mixed according to the mass ratio Sr:Ag = 1 − *X*:*X*, (*X* = 0, 1, 3, 5, 7, 9 %, respectively). First, the solid mixture was dissolved in 30 mL deionized water under magnetic stirring; Second, 2.4 mL tetrabutyl titanate was mixed with 30 mL absolute ethyl alcohol to form a clear solution; Thirdly, a certain amount of sodium hydroxide was added to 30 mL deionized water with magnetic stirring; the next step was to mix 14 mL oleic acid with 30 mL absolute ethyl alcohol via magnetic stirring; Finally, all of the above solution was transferred into a 170 mL of sealed Teflon-lined stainless-steel autoclave, which would be kept at 150 °C for 12 h and then cooled down to room temperature. The solid product was collected by centrifugal, washing with acetic acid, absolute ethyl alcohol and deionized water for three times respectively, and finally drying at 80 °C under vacuum.

2.2 Characterization of Catalysts

The crystal structure of the pristine and Ag-loaded $SrTiO_3$ powders were characterized by a Rigaku D X-ray powder diffractometer with Cu Kα radiation scanning from 10° to 80° at a scan rate of $2°min^{-1}$ and operating conditions of 40 kV and 150 mA. The $SrTiO_3$ crystallite size (D) was estimated by the Debye–Scherrer equation:

$$D = \frac{K\lambda}{\beta \cdot \cos\theta}$$

where *K* is the Scherrer constant (0.89), λ is the wavelength of the X-ray radiation (0.15418 nm for CuKa), β is the full width half maximum (FWHM) of the diffraction peak measured at 2θ, and θ is the diffraction angle. The photocatalyst morphologies and the existence of the loaded Ag were observed by a high-resolution transmission electron microscope (HRTEM: Tecnai G2 F20) at 200 kV. UV–Vis absorption spectra of the $SrTiO_3$ photocatalysts were obtained by using a UV–Vis diffuse reflectance spectroscopy (Shimadzu UV-2550) in wavelength of 200–800 nm at room temperature with $BaSO_4$ as a reference. Afterwards, the diffuse reflectance spectroscopy was used to estimate the band gap energy (*Eg*, eV) by using the Tauc equation:

$$(\alpha hv)^{1/2} = K(hv - Eg)$$

where *h* is the Planck's constant, *v* is the frequency of vibration, α is the absorption coefficient, *Eg* is the band gap (eV), *K* is the proportional constant. The unit for *hv* is eV (photon energy), and *hv* was determined by using the equation:

$$hv = \frac{1240}{\lambda}$$

λ is the wavelength (nm). The specific surface area of the $SrTiO_3$ photocatalysts was measured and calculated by a BET apparatus (APP V-Sorb 2800P) by nitrogen sorption at 77 K using the Brunauere–Emmette–Teller (BET) model. Mean pore size and distribution were determined by the Barrett–Joyner–Halenda (BJH) approach using the desorption data.

2.3 Photocatalytic Activity Evaluation

The photocatalytic reduction of CO_2 over the pristine $SrTiO_3$ and Ag–$SrTiO_3$ were evaluated in a batch slurry reactor showed in Fig. 1. A 250 W high-pressure mercury lamp was employed as UV light, whose main wavelength was 365 nm and 2800 $\mu W/cm^2$ illumination intensity reached the surface of the slurry. The photocatalytic activity evaluation was performed at 25 °C. To keep the reaction temperature constant, cooling water was recirculated through the jacket in outside of the quartz glass reactor. For each batch 20 mg photocatalyst was dispersed into 20 mL methanol by using a magnetic stirrer. CO_2 passed through the methanol at a flow rate of 100 mL/min for 30 min to approach the absorption equilibrium before irradiation. After ultraviolet light irradiation for 6 h, the product solution was qualitatively analyzed by GC–MS (Agilent 5975C) and quantitatively analyzed by gas chromatograph equipped with a hydrogen flame detector (FID). A ReactIR 15 (Mettler-Toledo, Switzerland) reaction analysis system equipped with a light fiber and Dicomp (diamond composite) insertion probe was used to collect FT-IR spectra of CO_2 in liquid. For comparison, the blank test was also carried out by irradiating the methanol without photocatalyst, or with photocatalyst in dark, the products were undetectable. This implied that the reaction depended on catalyst and light irradiation, indicating the reaction was a photocatalytic reduction process.

3 Results and Discussion

3.1 The XRD Analysis of $SrTiO_3$ and Ag–$SrTiO_3$ Photocatalysts

The crystal structures of synthesized $SrTiO_3$ and 7 wt% Ag–$SrTiO_3$ were analyzed by using XRD spectroscopy. As shown in Fig. 2, all the characteristic peaks, which refer to the single phase of cubic perovskite $SrTiO_3$, are in good agreement with the perovskite $SrTiO_3$ (JCPDS 35-0734, Cubic). Compared with the pristine $SrTiO_3$, an additional phase was identified to be the Ag (JCPDS 04-0783, Cubic) on the Ag-loaded $SrTiO_3$ photocatalyst. The peaks at 2θ = 38.116°, 44.277°, 64.426° and 77.472° belong to the

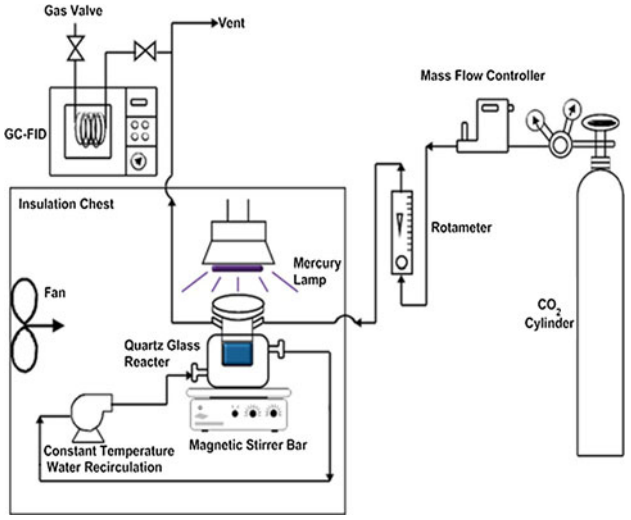

Fig. 1 Setup of photocatalytic reaction

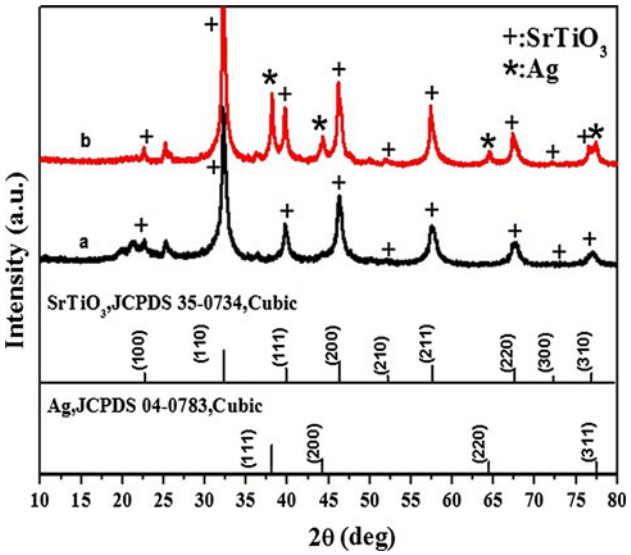

Fig. 2 X-ray diffraction patterns of *a* $SrTiO_3$, *b* 7 wt% Ag–$SrTiO_3$

characteristic peaks of Ag, which confirm that the Ag was loaded on the surface of perovskite $SrTiO_3$ and did not affect the crystallinity of the synthesized $SrTiO_3$ photocatalysts. The crystallite size of 7 wt% Ag–$SrTiO_3$ was calculated from the crystal plane (110) of $SrTiO_3$ diffraction peak by using the Debyee–Scherrer equation, which was nearly 19.8 nm, and the lattice spacing was 2.7776 Å. The contrasting data are listed in Table 1. Compared with the pristine $SrTiO_3$, there was negligible change in the Lattice Parameter for addition of Ag. The Lattice Parameter of $SrTiO_3$ measured from X-ray diffraction patterns was consistent to the JCPDS card. Furthermore, according to the UV–Vis DRS spectra results, the addition of Ag on the $SrTiO_3$ surface can enhance the light absorption ability and increase the band gap wavelength (λ) of the synthesized $SrTiO_3$ photocatalyst, leading to the decrease in the band gap energy from 2.85 to 2.28 eV (Table 1).

3.2 The SEM, TEM and HRTEM Observation of Ag–$SrTiO_3$ Photocatalyst

Morphologies of as-synthesized Ag–$SrTiO_3$ photocatalyst synthesized at different hydrothermal temperature and for different hydrothermal time were observed by SEM (Fig. 3). When the temperature reached 150 °C, the crystal was well crystallized and dispersed with uniform grain size (Fig. 3b). But at 170 °C, the crystal formed a structure of agglomeration, resulted in a low specific surface area and decrease in photocatalytic activity (Fig. 6c). SEM images Fig. 3(f–h) showed a partial collapse of crystal structure for crystallization period with a hydrothermal time for 28 h, which led to an extremely low specific surface area of 0.71 m^2/g (see BET result from Table 2).

Table 1 Textural properties of pristine and 7 wt% Ag-loaded $SrTiO_3$ from XRD and UV–Vis DRS analysis

Photocatalyst	Lattice plane[a]	Lattice parameter[a]	Lattice spacing[a] (A)	Crystallite size of $SrTiO_3$[a] (nm)	Eg[b] (eV)
Pristine $SrTiO_3$	110	0.3929	2.7759	16.0	2.85
7 wt% Ag–$SrTiO_3$	110	0.3931	2.7776	19.8	2.28

[a] From XRD analysis

[b] From UV–Vis DRS spectra analysis

In Fig. 3i, a TEM image of Ag–$SrTiO_3$ photocatalyst showed that a few black particles of silver was dispersed on the surface of the $SrTiO_3$. The particle size of Ag–$SrTiO_3$ is approximately 20 nm, which is quite in agreement with the XRD analysis. Figure 3j showed a HRTEM image of the same sample. The lattice plane of $SrTiO_3$ (110) with lattice spacing of 2.757 Å were clearly displayed, which were in accordance with the XRD analysis (shown in Table 1). It was clearly shown that the interface between $SrTiO_3$ and Ag changes continuously by forming an intergradation between $SrTiO_3$ and Ag. As indicated by the white loop, the interface between $SrTiO_3$ and Ag is conjunct well. The intergradation of the interface is beneficial in the transfer of the photogenerated electrons from the interior of $SrTiO_3$ to Ag in the reaction process [14, 15], and extend the life-span of the electron–hole pairs. The intergradation between the two particles has been found to be crucial for improving the photocatalytic activity.

3.3 The UV–Vis DRS Analysis of $SrTiO_3$ and Ag-Loaded $SrTiO_3$ Photocatalysts

Figure 4a showed the typical diffuse reflection spectra for the $SrTiO_3$ and Ag-loaded $SrTiO_3$ samples. Compared with the pristine $SrTiO_3$, Ag-loaded $SrTiO_3$ samples have a strong absorption in the visible light region, which is almost as strong as that in the UV region. This is attributed to the surface plasmon resonance of Ag nanoparticles deposited on $SrTiO_3$ particles [16–18]. Generally speaking, the surface plasmon absorption band of metal nanoparticles can be influenced by many factors such as particle size, particle shape, particle size distribution and surface charge density etc. The Ag nanoparticles deposited on $SrTiO_3$ particles have a large number of different shapes and diameters so that their plasmon oscillations cover a wide range of frequencies [19, 20]. Furthermore, surface plasmon absorption peak becomes broader and stronger with the increasing of hydrothermal time. It is the broader and stronger SPA peak that leads to an extension of the light absorption of the diffuse reflectance spectra of $SrTiO_3$. The presence of plasmon absorbance and the negligible change in the lattice parameters (as shown in Table 1) suggest that most of the metal exists as zerovalent metal deposits instead of substituting Sr or Ti sites within the perovskite structure [10]. This indicates that the main portion of the Ag added was present as zerovalent Ag. The absorption intensity of the diffuse reflectance spectra of Ag–$SrTiO_3$ is dependent on the synthesis times, which give rise to an extension of the light absorption with the increase of synthesis times. Theoretically speaking, when the absorption intensity via UV–Vis analysis increases, the generation of electron–hole pairs increases, resulting in the photocatalyst exhibiting a higher photocatalytic activity.

As shown in Fig. 4b, the intercept of the tangent to the square root of the Kubelka–Munk functions $(\alpha h\nu)^{1/2}$ versus the photon energy ($h\nu$) plots would give an estimation of the band gap for indirect bandgap semiconductors such as $SrTiO_3$. When the tangent lines are extrapolated to $\alpha^{1/2} = 0$, the band gaps of pristine $SrTiO_3$ and 7 wt% Ag–$SrTiO_3$ on hydrothermal time for 10, 16, 22 and 28 h are indicated to be 2.85, 2.28, 2.28, 1.79, and 1.12 eV respectively. The band gap energy of pristine $SrTiO_3$ is larger than that of 7 wt% Ag loaded $SrTiO_3$. And it is evident that the band gap energies of Ag–$SrTiO_3$ on different hydrothermal time decreased with the increasing hydrothermal time. Thus, 7 wt% Ag–$SrTiO_3$ might absorb light in a larger wavelength region up to visible light.

3.4 The BET Specific Surface Area Analysis of $SrTiO_3$ and Ag-Loaded $SrTiO_3$ Photocatalysts

The porous structure of the pristine $SrTiO_3$ and 7 wt% Ag–$SrTiO_3$ had been identified by the N_2 sorption isotherms, as shown in Fig. 5. The isotherms showed a type IV IUPAC pattern with a hysteresis loop, demonstrating that the pristine $SrTiO_3$ and 7 wt% Ag–$SrTiO_3$ consist of well-developed mesopores ($2.0\ \text{nm} < d_p \leq 50\ \text{nm}$) in their assembled frameworks. From the BJH pore diameter distributions, as shown in Fig. 5 inset, it is evident that the Ag loaded $SrTiO_3$ possessed a similar pore diameters with the pristine $SrTiO_3$. The N_2 absorption–desorption analysis results showed that the Ag loading increased the specific surface area and total pore volume, and possessed a similar mean pore diameter to the pristine $SrTiO_3$. The BET specific surface area of the Ag loaded $SrTiO_3$ samples were investigated as summarized in Table 2. We focused on the Ag loaded $SrTiO_3$ with a much larger surface area than the pristine $SrTiO_3$ particles. As for the specific surface area of the Ag loaded $SrTiO_3$ samples on different synthesis temperature, when the temperature reached 150 °C, the surface area of the catalyst became the largest, which is possibly because the crystal synthesized at 150 °C are well crystallized and dispersed with uniform grain size, which is in well agreement with the SEM analysis, as shown in Fig. 3b. As shown in Fig. 6c for the photocatalytic activities analysis, the Ag–$SrTiO_3$ prepared at 150 °C showed the highest activity. Therefore, 150 °C is considered the optimum hydrothermal temperature. The surface area of the crystal decreased as the Ag dosage increased below 5 wt%, and increased at 7 and 9 wt%, as shown in Table 2. Furthermore, the specific surface area of the 7 wt% Ag–$SrTiO_3$ crystal increased as the hydrothermal time increased below 22 h, but the specific surface area sharply decreased when the time increased to 28 h, possibly due to a collapse of crystal structure for crystallization period with a hydrothermal time for 28 h. The result is quite in accordance with the SEM analysis (shown in Fig. 3h). The photocatalyst with high specific surface area exhibited the enhanced activity, which is ascribed to more reaction sites arising from high specific surface area, and the efficient transition of the photogenerated electron–hole pairs to the surface. For all that, the relatively small specific surface area for our samples suggested that surface area could not be the decisive factor for its high activity.

3.5 Photocatalytic Activities of $SrTiO_3$ and Ag-Loaded $SrTiO_3$ Photocatalysts for Reduction of CO_2

The Photocatalytic activities of as-synthesized Ag-loaded $SrTiO_3$ samples during photocatalytic reduction of CO_2 under irradiation were evaluated. For the sake of the improvement of photocatalytic activity, the optimization of the operational parameters for the CO_2 reduction system is important. In our work, the effects of Ag dosage, time and temperature of hydrothermal synthesis on the photocatalytic activity were investigated. As shown in Fig. 6a,

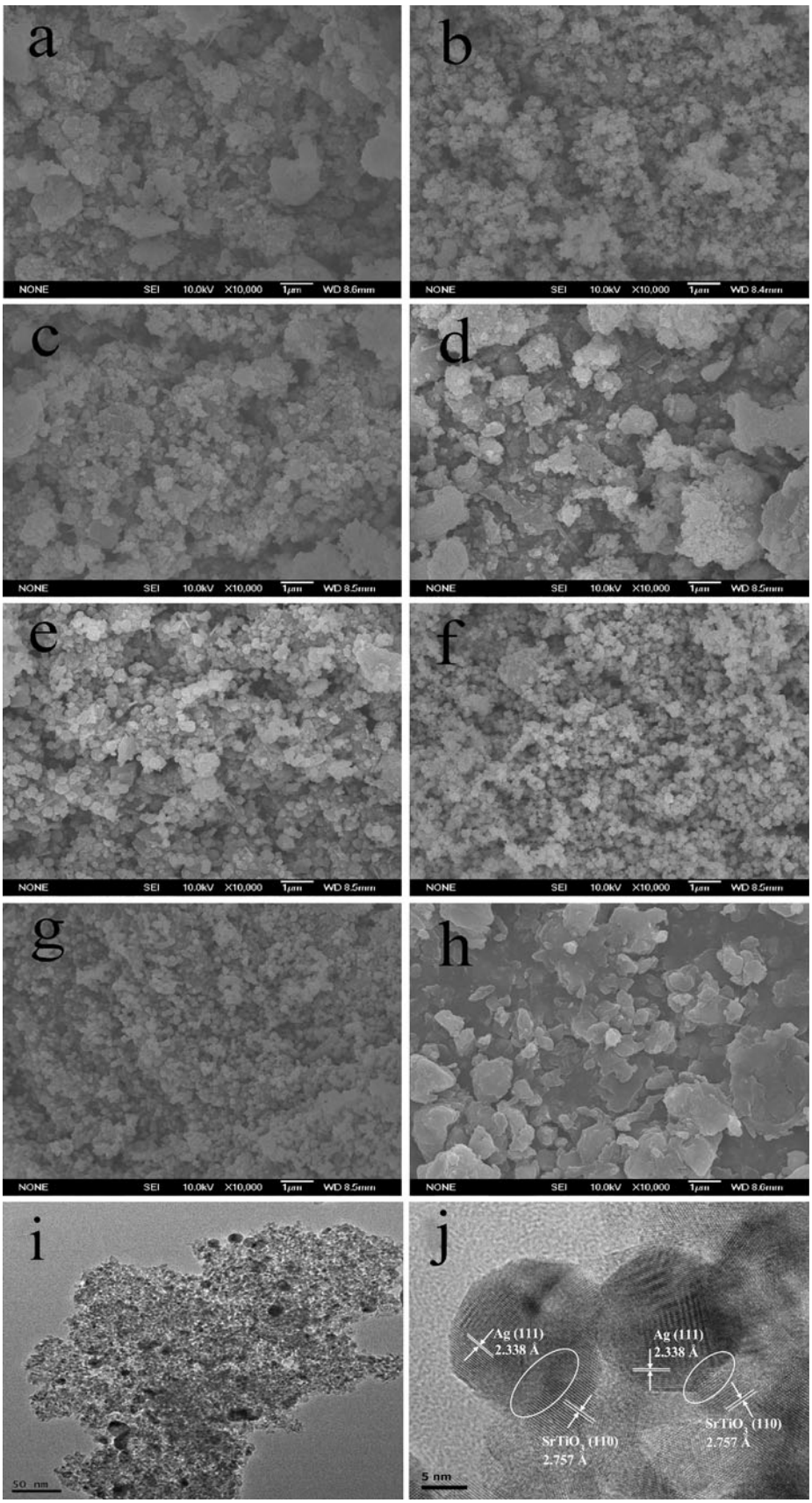

Fig. 3 SEM images of 7 wt% Ag–$SrTiO_3$ samples: **a–e** the samples synthesized at 140, 150, 160, 170 and 180 °C for 10 h, **f–h** the samples synthesized for 16, 22 and 28 h at 150 °C, **i** TEM image of 7 wt% Ag–$SrTiO_3$ (150 °C, 10 h), **j** HRTEM image of 7 wt% Ag–$SrTiO_3$ (150 °C, 10 h)

Table 2 The surface area of Ag-loaded $SrTiO_3$ photocatalysts

Photocatalyst	Dosage of Ag (wt%) loaded on $SrTiO_3$ at 150 °C for 10 h						7 wt% Ag–$SrTiO_3$, 150 °C synthesis time (h)				7 wt% Ag–$SrTiO_3$, 10 h synthesis temperature (°C)				
	0	1	3	5	7	9	10	16	22	28	140	150	160	170	180
BET specific surface area (m^2/g)	1.85	18.88	12.10	7.11	13.81	10.68	13.81	14.46	23.78	0.71	7.16	13.81	10.81	3.46	9.20

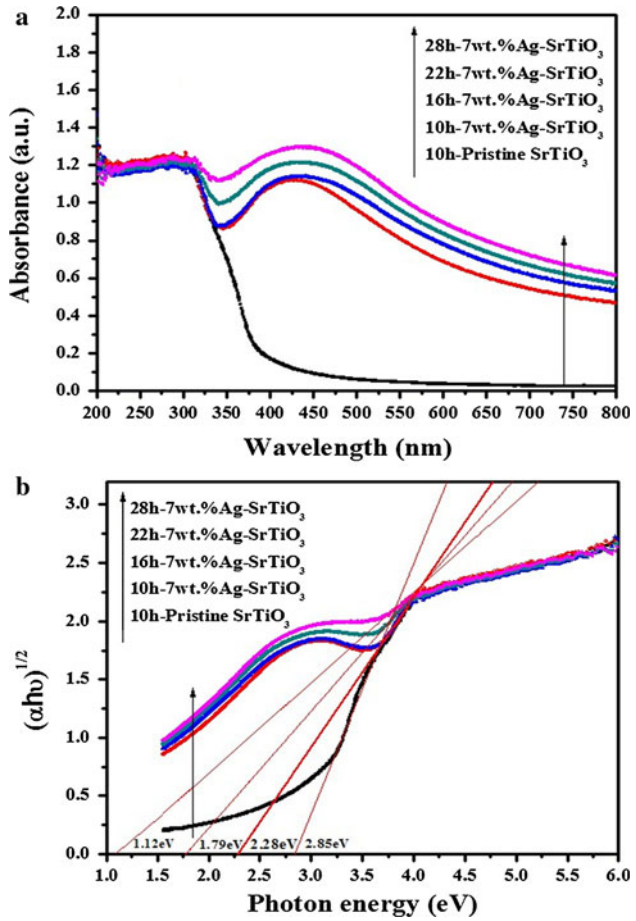

Fig. 4 **a** UV–Vis DRS spectra of pristine $SrTiO_3$ and 7 wt% Ag–$SrTiO_3$ for different hydrothermal time. **b** Plots of $(\alpha hv)^{1/2}$ versus photon energy (hv) for pristine $SrTiO_3$ and 7 wt% Ag–$SrTiO_3$ on different hydrothermal times

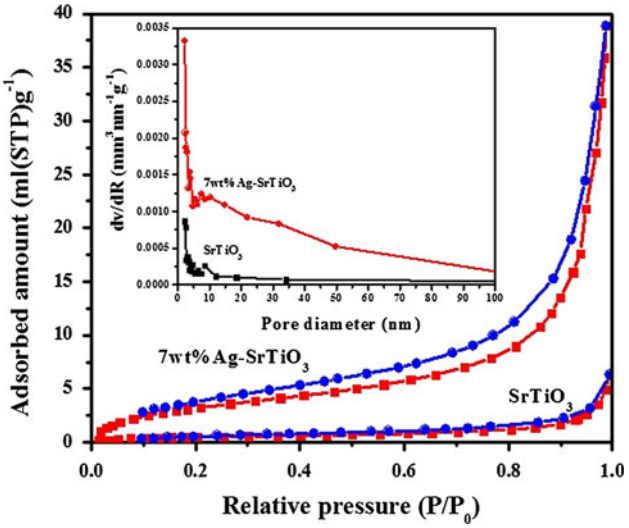

Fig. 5 N_2 sorption isotherms and pore diameter distributions (*inset*) of the pristine and the 7 wt% Ag-loaded $SrTiO_3$ photocatalysts

increasing loaded Ag from 0 to 7 wt% gave rise to an increase in the MF evolution rate. In our experimental range, the increase of the surface area of the Ag particles with increasing loaded Ag could result in a positive evolution rate of MF. As the Ag increased from 1 to 5 wt%, the specific surface area decreased abruptly in spite of the increasing MF evolution rate. Nevertheless, a further increase in the Ag loading (higher than 9 wt%) led to a decrease in rate of MF evolution, which should be ascribed to the excess Ag agglomeration acting as the electron–hole recombination center, resulting in a negative activity effect [7, 21, 22] .

The effect of hydrothermal time and hydrothermal temperature on photocatalytic activity was shown in Fig. 6b, c. In Fig. 6b, for the hydrothermal time from 10 to 22 h, the increase of hydrothermal time led to an increase in the crystallinity and the specific surface area [8], which resulted in the positive effect on photocatalytic activity. However, for the hydrothermal time from 22 to 28 h, the increase in the hydrothermal time led to a slight increase in the crystallinity but an abrupt decrease in the specific surface area. In this time range, the decrease of the photocatalytic activity possibly due to the negative effect of the specific surface area might surpass the positive effect of crystallinity. The effect of hydrothermal temperature can be divided into three sections, as shown in Fig. 6c. Firstly, for the hydrothermal temperature from 140 to 150 °C, the increase hydrothermal time led to an increase in the crystallinity and the specific surface area, which resulted in the positive photocatalytic activity. Secondly, for the hydrothermal temperature from 150 to 170 °C, the increase in the hydrothermal temperature led to a slight increase in the crystallinity but a decrease in the specific surface area. In this time range, the photocatalytic activity possibly due to

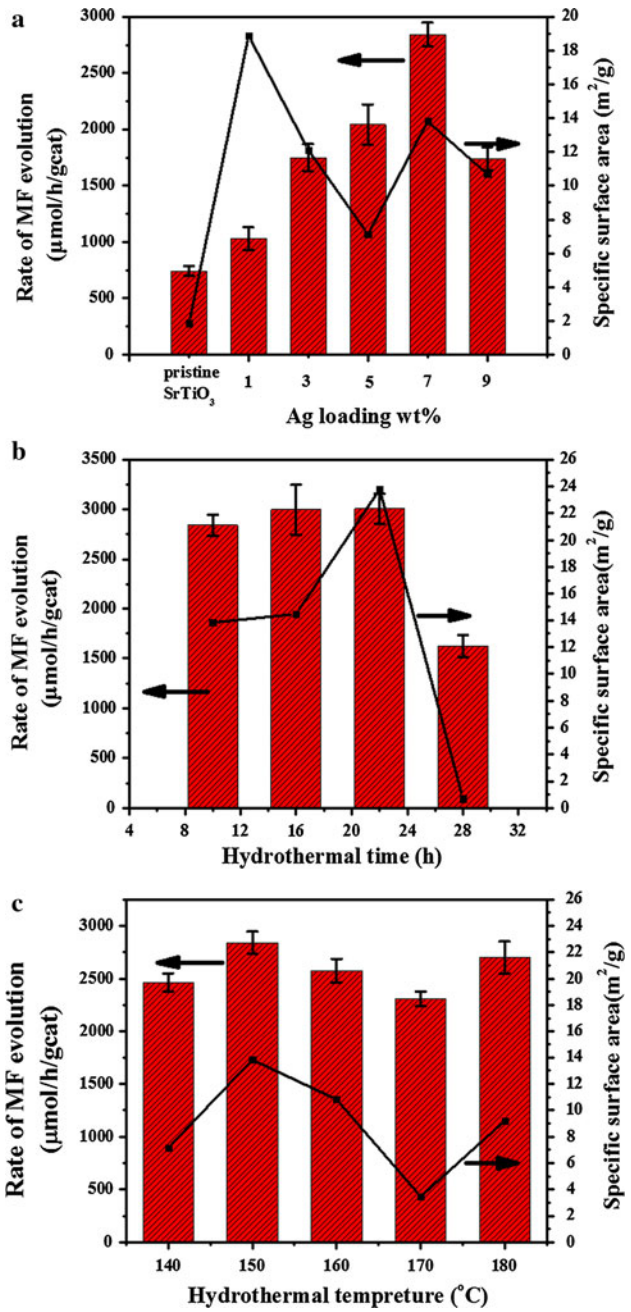

Fig. 6 **a** The rate of MF evolution and specific surface area of Ag loaded $SrTiO_3$ (a hydrothermal temperature of 150 °C, a hydrothermal time of 10 h) on different Ag loading wt%. **b** The rate of MF evolution and specific surface area of 7 wt% Ag–$SrTiO_3$ (a hydrothermal temperature of 150 °C) on different hydrothermal time. **c** The rate of MF evolution and specific surface area of 7 wt %Ag–$SrTiO_3$ (a hydrothermal time of 10 h) on different hydrothermal temperature

the negative effect of the specific surface area might surpass the positive effect of crystallinity. Thirdly, for the hydrothermal temperature from 170 to 180 °C, the increase hydrothermal temperature resulted in an increase of the crystallinity and the specific surface area, which led to the enhanced photocatalytic activity.

The photocatalytic activities of the Ag loaded $SrTiO_3$ photocatalysts strongly depended on the light absorbance of $SrTiO_3$ powders, the Ag loading on $SrTiO_3$, the hydrothermal synthesis condition, which resulted in corresponding variation in the specific surface area and crystallinity, affecting their photocatalytic activities.

For monitoring the conversion of CO_2 in methanol, we employed the on line ReactIR to collect FT-IR spectra of CO_2 in liquid phase by using a AgX optic probe inserted into the reactor. After CO_2 bubbled through the methanol solution the IR spectra are shown in Fig. 7. From the 3D plots in Fig. 7a, we noted that CO_2 at 2,342 cm^{-1} was captured. The peak area of CO_2 versus time in Fig. 7b clearly showed the conversion of CO_2. In the presence of ultraviolet illumination, the CO_2 was obviously consumed, but turning off the light, the concentration of CO_2 remained almost stable. It is, therefore, noteworthy that CO_2 was directly involved in the reaction.

3.6 Mechanism of Photocatalysis

The mechanism for photocatalytic reduction of CO_2 to methyl formate in methanol was shown in Fig. 8. When the $SrTiO_3$ is irradiated by UV light of suitable wavelength with sufficient photonic energy (hv), photo-generated electron–hole pairs were created, part of the excited electrons and holes recombined together and radiated out heat, while rest part would react with the reactants near the $SrTiO_3$ surface. It was certain electrons transmitting to the surface of Ag particle that avoided their recombination with holes, resulting in effective extension of the life-span of the electron–hole pairs. In the process, the Ag particle acted as electron acceptor. The potential energy of conduction band of $SrTiO_3$ is −1.26 V, which is more negative than that of CO_2/formic acid or formaldehyde, and the potential energy of valence band of 2.14 V is more positive than that of methanol oxidation [23, 24]. The excited electrons reacted with the CO_2 adsorbed on the catalyst surface to produce formic acid or formaldehyde, at mean time, the excited holes reacted with the CH_3OH to produce formaldehyde and formic acid. The methyl formate product can be generated through the esterification of formic acid and methanol and the dimerization of formaldehyde via Tishchenko reaction.

In a comparison experiment, 7 wt% Ag–$SrTiO_3$ (150 °C, 22 h) was used to investigated the effect of CO_2. A test bubbling the solution with N_2 instead of CO_2 was performed. It turned out that, in the presence of CO_2, MF generation rate was 3006 mol/(h g cat), while in the presence of N_2, MF generation rate was 925 mol/(h g cat). When CO_2 was substituted for N_2, MF was generated through the dimerization of formaldehyde via Tishchenko reaction, but the amount was less than one-third of that in

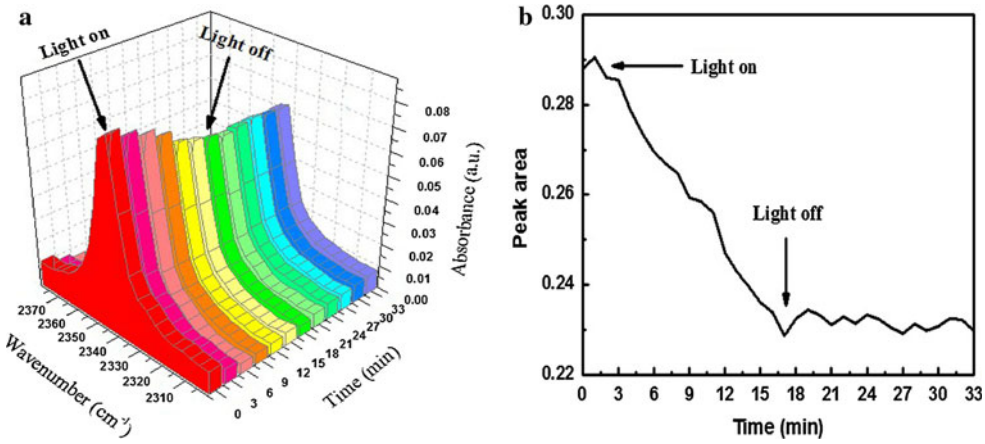

Fig. 7 **a** 3D plots of on line ReactIR spectra for the reaction, (**b**) peak area of CO_2 at 2,342 cm^{-1}

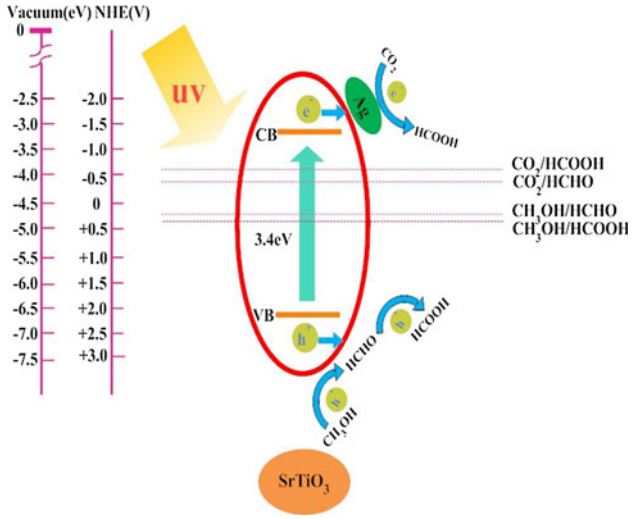

Fig. 8 Schematic mechanism of UV photocatalytic reduction of CO_2 over Ag–$SrTiO_3$

the presence of CO_2. This indicated that CO_2 was reduced to HCOOH and HCHO in the CB and made a main contribution to the MF generation [25].

4 Conclusions

Pristine and Ag-loaded $SrTiO_3$ nanocrystal photocatalysts had been prepared via hydrothermal synthesis method. The absorption edge of as-synthesized photocatalyst was evidently extended up to visible light by Ag-loading. The photocatalytic activities could be further enhanced via extending life-span of the electron–hole pairs by using Ag particle as electron acceptor. The optimum loading dosage of Ag is 7 wt%, hydrothermal temperature of 150 °C and a hydrothermal time of 22 h. The prepared photocatalysts displayed a high activity for the reduction of CO_2 in methanol to methyl formate, the highest MF evolution rate reached 3,006 μmol/(h g cat).

Acknowledgments We gratefully acknowledge financial support by the National Natural Science Foundation of China (NSFC) (No. 21176192) and the Tianjin natural science foundation (No. 12JCZDJC29400).

References

1. Ahmed N, Shibata Y, Taniguchi T, Izumi Y (2011) J Catal 279:123
2. Kitano M, Matsuoka M, Ueshima M, Anpo M (2007) Appl Catal A 325:1
3. Chen L, Graham ME, Li G, Gentner DR, Dimitrijevic NM, Gray KA (2009) Thin Solid Films 517:5641
4. Dey GR, Belapurkar AD, Kishore K (2004) J Photochem Photobiol A Chem 163:503
5. Nasution H, Purnama E, Kosela S, Gunlazuardi J (2005) Catal Commun 6:313
6. Tseng IH, Wu JCS (2004) Catal Today 97:113
7. Puangpetch T, Sreethawong T, Chavadej S (2010) Int J Hydrogen Energy 35:6531
8. Puangpetch T, Sreethawong T, Yoshikawa S, Chavadej S (2008) J Mol Catal A Chem 287:70
9. Qin Y, Wang G, Wang Y (2007) Catal Commun 8:926
10. Subramanian V, Roeder RK, Wolf EE (2006) Ind Eng Chem Res 45:2187
11. Wang J, Yin S, Komatsu M, Zhang Q, Saito F, Sato T (2004) J Photochem Photobiol A Chem 165:149
12. Sun Y, Liu J, Li Z (2011) J Solid State Chem 184:1924
13. Puangpetch T, Sreethawong T, Yoshikawa S, Chavadej S (2009) J Mol Catal A Chem 312:97
14. Ma BJ, Yang JH, Han HX, Wang JT, Zhang XH, Li C (2010) J Phys Chem C 114:12818
15. Yu J, Xiong J, Cheng B, Liu S (2005) Appl Catal B Environ 60:211
16. Jia A, Su Z, Lou L-L, Liu S (2010) Solid State Sci 12:1140
17. Linic S, Christopher P, Ingram DB (2011) Nat Mater 10:911
18. Wang P, Huang B, Zhang Q, Zhang X, Qin X, Dai Y, Zhan J, Yu J, Liu H, Lou Z (2010) Chemistry 16:10042
19. Jain PK, Huang W, El-Sayed MA (2007) Nano Lett 7:2080
20. Wang P, Huang B, Zhang X, Qin X, Jin H, Dai Y, Wang Z, Wei J, Zhan J, Wang S, Wang J, Whangbo MH (2009) Chemistry 15:1821
21. Liu J, Sun Y, Li Z, Li S, Zhao J (2011) Int J Hydrogen Energy 36:5811

22. Jing D, Liu M, Chen Q, Guo L (2010) Int J Hydrogen Energy 35:8521
23. Chen X, Shen S, Guo L, Mao SS (2010) Chem Rev 110:6503
24. Xu Y, Schoonen MAA (2000) Am Mineral 85:543
25. Qin S, Xin F, Liu Y, Yin X, Ma W (2011) J Colloid Interface Sci 356:257